JACS
JOURNAL OF THE AMERICAN CHEMICAL SOCIETY
pubs.acs.org/JACS
Article

Chemical and Structural Evolution of AgCu Catalysts in Electrochemical CO_2 Reduction

Peng-Cheng Chen,[#] Chubai Chen,[#] Yao Yang,[#] Arifin Luthfi Maulana, Jianbo Jin, Julian Feijoo, and Peidong Yang*

Cite This: J. Am. Chem. Soc. 2023, 145, 10116−10125

ABSTRACT: Silver−copper (AgCu) bimetallic catalysts hold great potential for electrochemical carbon dioxide reduction reaction (CO_2RR), which is a promising way to realize the goal of carbon neutrality. Although a wide variety of AgCu catalysts have been developed so far, it is relatively less explored how these AgCu catalysts evolve during CO_2RR. The absence of insights into their stability makes the dynamic catalytic sites elusive and hampers the design of AgCu catalysts in a rational manner. Here, we synthesized intermixed and phase-separated AgCu nanoparticles on carbon paper electrodes and investigated their evolution behavior in CO_2RR. Our time-sequential electron microscopy and elemental mapping studies show that Cu possesses high mobility in AgCu under CO_2RR conditions, which can leach out from the catalysts by migrating to the bimetallic catalyst surface, detaching from the catalysts, and agglomerating as new particles. Besides, Ag and Cu manifest a trend to phase-separate into Cu-rich and Ag-rich grains, regardless of the starting catalyst structure. The composition of the Cu-rich and Ag-rich grains diverges during the reaction and eventually approaches thermodynamic values, i.e., $Ag_{0.88}Cu_{0.12}$ and $Ag_{0.05}Cu_{0.95}$. The separation between Ag and Cu has been observed in the bulk and on the surface of the catalysts, highlighting the importance of AgCu phase boundaries for CO_2RR. In addition, an operando high-energy-resolution X-ray absorption spectroscopy study confirms the metallic state of Cu in AgCu as the catalytically active sites during CO_2RR. Taken together, this work provides a comprehensive understanding of the chemical and structural evolution behavior of AgCu catalysts in CO_2RR.

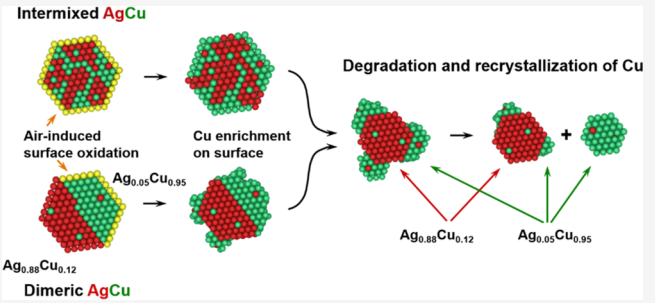

INTRODUCTION

Electrochemical carbon dioxide reduction reaction (CO_2RR), with the capability of utilizing CO_2 as a feedstock to generate value-added chemicals, has the promise to lessen the dependence on fossil fuels and decouple CO_2 emissions from economic growth, thus attracting broad interest in recent years.[1−6] Thus far, Cu is the only monometallic catalyst that can effectively convert CO_2 to multicarbon products, which becomes the most important catalytic system for electrochemical CO_2RR. However, the Cu system alone is not ideal for transforming CO_2 to CO and thereby limits the subsequent generation of multicarbon products.[6−8] One strategy to improve the CO_2RR performance of Cu is to construct a multimetallic system, where Cu and the other metal components can function synergistically.[9−26] Specifically, the synergistic effects can be realized through the electron richness/deficiency of the copper surface induced by the Fermi level differences between heterogeneous metals,[13] the intrinsic stress and surface reconstruction caused by heterogeneous atoms,[14,15] the newly introduced asymmetric catalytic sites,[16] or the tandem effect.[17−19] Under this framework, multiple elements such as Pd,[20,21] Au,[13,22] Zn,[23−25] and Al[26] have been confirmed to have positive promoting effects on the Cu-based CO_2RR catalytic system. Notably, Ag appears to be a promising candidate metal for a Cu-based bimetallic catalytic system because of its high efficiency of generating CO from CO_2[27,28] and its thermodynamic immiscibility with Cu.[29−32] In view of its potential, many efforts have been made on developing silver−copper (AgCu) bimetallic catalysts for CO_2RR.

Based on the interaction between Cu and Ag, AgCu bimetallic catalysts can be classified into three categories. In the first group, Ag and Cu are physically mixed to form tandem catalysts where Ag creates a CO-concentrated local environment that can be utilized by Cu to boost the generation rate of multicarbon products.[17−19,33] Inspired by this design principle, in the second category, AgCu nanostructures that are rich in

Received: January 13, 2023
Published: April 28, 2023

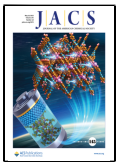

https://doi.org/10.1021/jacs.3c00467
J. Am. Chem. Soc. 2023, 145, 10116−10125

phase boundaries between Cu and Ag have been devised to further enhance the spillover of CO from the Ag sites to the Cu surface.[34−39] Finally, even though Cu and Ag are highly immiscible metals,[29] the mixing energy change caused by the large surface area of nanostructures makes the slight alloying between Cu and Ag possible at the nanoscale.[40] Therefore, multiple strategies have been established to introduce Ag atoms into the Cu phase, such as galvanic replacement,[14,41] co-sputtering,[16] ligand-assisted co-deposition,[42] oxidation/reduction-driven atomic interdiffusion,[15] and thermal shock synthesis.[43] Although a wide range of AgCu catalysts have been successfully made for CO_2RR, surprisingly, the chemical and structural evolution of AgCu is barely investigated despite the fact that catalysts are often unstable under the electrochemical environment.[44−47] For example, Cu catalysts have been reported to be highly mobile under the CO_2RR environment, which will form active nanograins via structural evolution of the catalysts.[46,48−52] Given the high mobility of Cu and the large immiscibility between Ag and Cu, it is possible that AgCu catalysts will evolve under the CO_2RR environment. Considering the rich chemistry of Cu and Ag at the nanoscale that will principally make the further optimization of AgCu catalysts feasible, understanding the chemical and structural fate of AgCu electrocatalysts will be crucial for the design of novel AgCu and other multimetallic catalysts with superior activity and stability.

Herein, we synthesized two types of AgCu catalysts, i.e., intermixed and phase-separated AgCu particles, and systematically explored their evolution behavior in CO_2RR. We found that the two types of catalysts evolve into similar structures primarily due to the high mobility of Cu under the CO_2RR conditions (Figure 1). For intermixed AgCu catalysts, Cu will

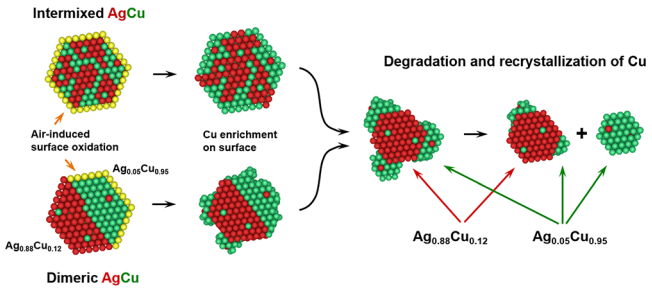

Figure 1. Schematic illustration of the chemical and structural evolution of intermixed and phase-separated AgCu catalysts in electrochemical CO_2RR.

leach out from the catalysts during CO_2RR, which is subsequently enriched on the particle surface or recrystallized elsewhere as new particles. For phase-separated AgCu catalysts, the Cu domains are corroded during CO_2RR and migrate to the Ag domain surface, resulting in structures similar to what has been observed in the intermixed AgCu case. While Ag and Cu generally tend to phase-separate as the reaction proceeds owing to their high immiscibility, the two elements are still slightly mixable to form Ag-rich and Cu-rich domains in the nanocatalysts within the thermodynamic solubility limit.

RESULTS AND DISCUSSION

The intermixed AgCu nanoparticles (NPs) were prepared by microwave-assisted shock synthesis. Experimentally, carbon paper substrates loaded with Ag and Cu salt precursors were first irradiated by microwave to instantly raise the temperature to higher than 1000 °C.[53] This high temperature will thermally decompose the salt precursors while allowing Ag and Cu to be mixed in a liquid state (Figure S1). The elemental mixture was then quenched by rapid cooling when the irradiation was turned off to yield the intermixed AgCu particles. As shown in Figures 2a and S2, AgCu NPs with sizes between 10 and 100 nm were successfully synthesized via this method. Energy-dispersive X-ray spectroscopy (EDS) analysis confirms that the NPs have an average composition of $Ag_{0.5}Cu_{0.5}$, and the two elements seem evenly distributed in the NPs. However, magnified EDS mapping of individual NPs reveals that the particles are indeed composed of Cu-rich and Ag-rich grains of size smaller than 10 nm (Figure S3), rather than forming a single-phase AgCu mixture. The co-existence of Ag-rich and Cu-rich phases was further corroborated by X-ray diffraction (XRD) characterization (Figure 2b), which exhibits two sets of diffraction peaks that can be assigned to the two phases, respectively. The diffraction peaks were found to slightly shift when compared with the standard peaks of monometallic Cu and Ag, suggesting that the two phases are not compositionally pure. Ag and Cu are inter-doped in these Ag-rich and Cu-rich grains. Furthermore, high-resolution transmission electron microscopy (HRTEM) characterization was carried out to gain more insights into the particle structure at an individual particle level. As shown in Figures 2c and S4, the AgCu NPs have an fcc lattice structure. Fast Fourier transform (FFT) of the selected area confirms the presence of Ag-rich and Cu-rich lattices. In some particles, the two types of grains are coherently oriented, and moiré patterns with a 1.82 nm spacing can be observed due to the periodical lattice matching between the Ag(111) and Cu(111) planes. In addition, an ∼2 nm oxide layer can be found on the NP surface, likely caused by Cu oxidation upon exposing the particle to air. Collectively, these characterizations confirm that the as-synthesized $Ag_{0.5}Cu_{0.5}$ NPs consist of a mixture of Ag-rich and Cu-rich grains (<10 nm), i.e., a phase-blended structure. For simplicity, we name this AgCu phase-blended structure as intermixed AgCu (I-AgCu) in the following text.

Electrochemical CO_2RR was performed on the as-synthesized I-AgCu NPs in a 0.1 M $KHCO_3$ electrolyte using a three-electrode system in conventional H-cells. Considering that the evolution behavior of monometallic Cu under CO_2RR has been reported to strongly relate to the applied potential as well as the binding intermediates,[45−48,54−56] we chose a moderate potential (−1.0 V vs RHE) as a representative condition to conduct the CO_2RR. Under this reaction potential, the Faraday efficiency toward hydrogen evolution reaction and CO_2RR is roughly equal (Figure S5 and Table S1). High-angle annular dark-field scanning transmission electron microscopy (HAADF-STEM) and EDS characterizations were performed on the AgCu catalysts that have catalyzed CO_2RR for a specific time between 0 and 24 h. As shown in Figure 3a, Cu and Ag exhibit a trend to separate from each other during the reaction. After 0.5 h of electrolysis, enrichment of Cu species on the catalyst surface can already be observed (Figure 3a, second column). When the electrolysis time is extended to 1 or 3 h, more Cu species are leached out and migrate to the catalyst surface, leading to a thicker layer of Cu on the particles (Figure 3a, third and fourth columns). Meanwhile, some Cu particles (<5 nm) are detached from the parental AgCu catalysts (Figure S6). When the reaction time is further prolonged to 6 h, individual Cu particles with size >10 nm and are not in

https://doi.org/10.1021/jacs.3c00467
J. Am. Chem. Soc. 2023, 145, 10116−10125

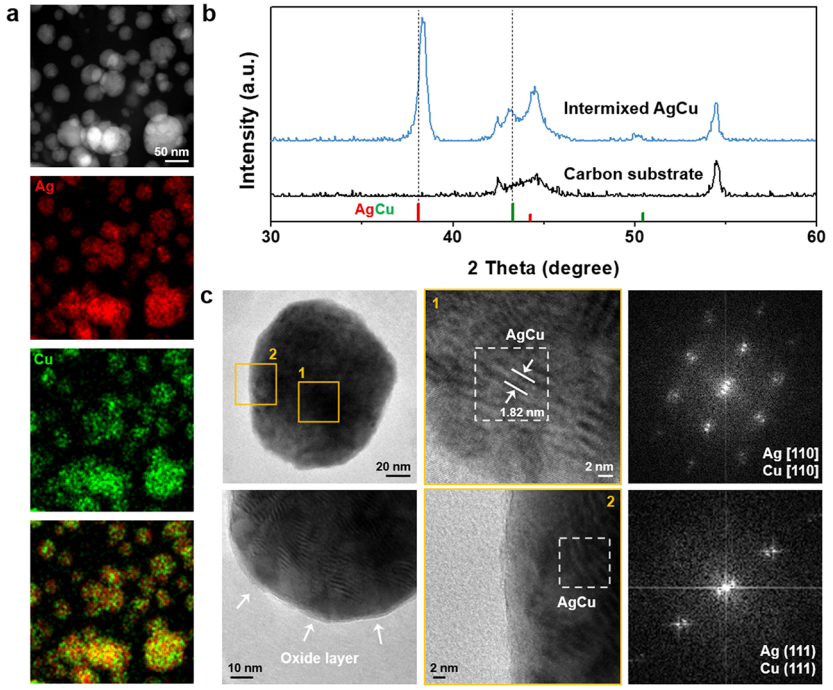

Figure 2. Structural characterization of intermixed AgCu catalysts made by microwave-assisted shock synthesis. (a) HAADF-STEM image and EDS elemental mapping of intermixed $Ag_{0.5}Cu_{0.5}$ particles synthesized on carbon paper substrates. (b) XRD patterns of the carbon paper substrates and the as-synthesized I-AgCu particles. (c) HRTEM characterization of the I-AgCu particles. The orange squares in the first image denote the zoomed-in regions for imaging, which are shown in the second column. The white dashed squares in the second column of images indicate the areas selected for FFT analysis. The FFT results are shown in the third column.

proximity to the original AgCu particles can be observed (Figure 3a, fifth column), which are presumably formed by the coalescence of the detached Cu particles. After 24 h of electrolysis, Cu is severely segregated from Ag, either forming large-size grains that still stick to the original particles or agglomerating elsewhere as new particles (Figure 3a, last column, and Figure S7). The structural evolution of the I-AgCu catalysts is also reflected in their XRD patterns (Figure 3b). It can be seen that the (111) peak assigned to the Cu-rich grains is flattened when the reaction starts due to the reduced crystallinity of Cu when it degrades from the catalysts. Moreover, the (111) peak belonging to the Ag-rich grains gradually shifts to lower-angle positions after the electrolysis, suggesting the leaching of the Cu dopants from the Ag-rich grains during the reaction. However, even after 24 h of electrolysis, the (111) peak position of Ag-rich grains is higher than that of standard Ag, indicating that there is still a certain amount of Cu doped in the Ag-rich grains. Ex situ HRTEM characterization further supports the structural evolution behavior of the catalysts (Figures 3c and S4). Before the electrolysis, a 2 nm air-induced Cu_2O layer can be observed through HRTEM. After 3 h of reaction, larger Cu_2O grains (2−8 nm) were developed on the catalyst surface. Further extending the electrolysis time results in larger-size Cu domains that are observable under HRTEM. It should be noted that although we observe Cu_2O lattices in the catalysts that were taken out from the reaction, these oxides are formed because of the air exposure after electrolysis. Our operando X-ray absorption spectroscopy (XAS) study in the following text has proven that the Cu species maintain a metallic state under the reaction environment. Compared with the poor stability of Cu in CO_2RR, Ag is much less mobile in CO_2RR, as evidenced by the minor change of the Ag-containing particle size (Figure S8). Taken together, it is clear that the Cu and Ag in the intermixed AgCu particles will structurally separate from each other during CO_2RR. Cu species migrate to the catalyst surface and grow into large-size grains or detach from the catalyst surface and agglomerate as new particles.

To further elucidate the separation state between Ag and Cu during CO_2RR, in particular, whether the two elements have been completely separated as suggested by the phase diagram, we conducted a compositional analysis on the Ag-rich and Cu-rich phases using a combination of XRD, selected area electron diffraction (SAED), and EDS (Figure 4). For the Ag-rich phases, the d-spacing of (111) planes is gradually increased when the electrolysis proceeds, but it remains smaller than that of pure Ag, as evidenced by both XRD characterization of the catalyst ensemble and SAED analysis of selected NPs (Figures 4b,c and S9). The results confirm the leach-out of Cu from the original Ag-rich phase until a new stable Ag-rich phase with a lower Cu content is established. EDS analysis was utilized to quantify the composition of the entire particle catalyst, the Ag-rich domain, and the leached Cu domain. As shown in Figures 4d,e and S10, the Cu content in the Ag-rich domain decreases until a steady state containing ∼12% of Cu is achieved after ∼3 h of electrolysis. This specific composition, $Ag_{0.88}Cu_{0.12}$, can be considered as the thermodynamically stable composition of the Ag-rich phase under CO_2RR conditions. Within a similar reaction time, the Cu content of the leached Cu domain increases to ∼95%. Therefore, Ag and Cu are not fully separated from each other in CO_2RR. The original I-AgCu is converted from a metastable state to thermodynamically stable Ag-rich and Cu-rich phases that can be denoted as $Ag_{0.88}Cu_{0.12}$ and $Ag_{0.05}Cu_{0.95}$, respectively. In the meantime, we found that the Cu content of the entire Ag-containing particles is continuously decreased during the electrolysis. Given the low

https://doi.org/10.1021/jacs.3c00467
J. Am. Chem. Soc. 2023, 145, 10116−10125

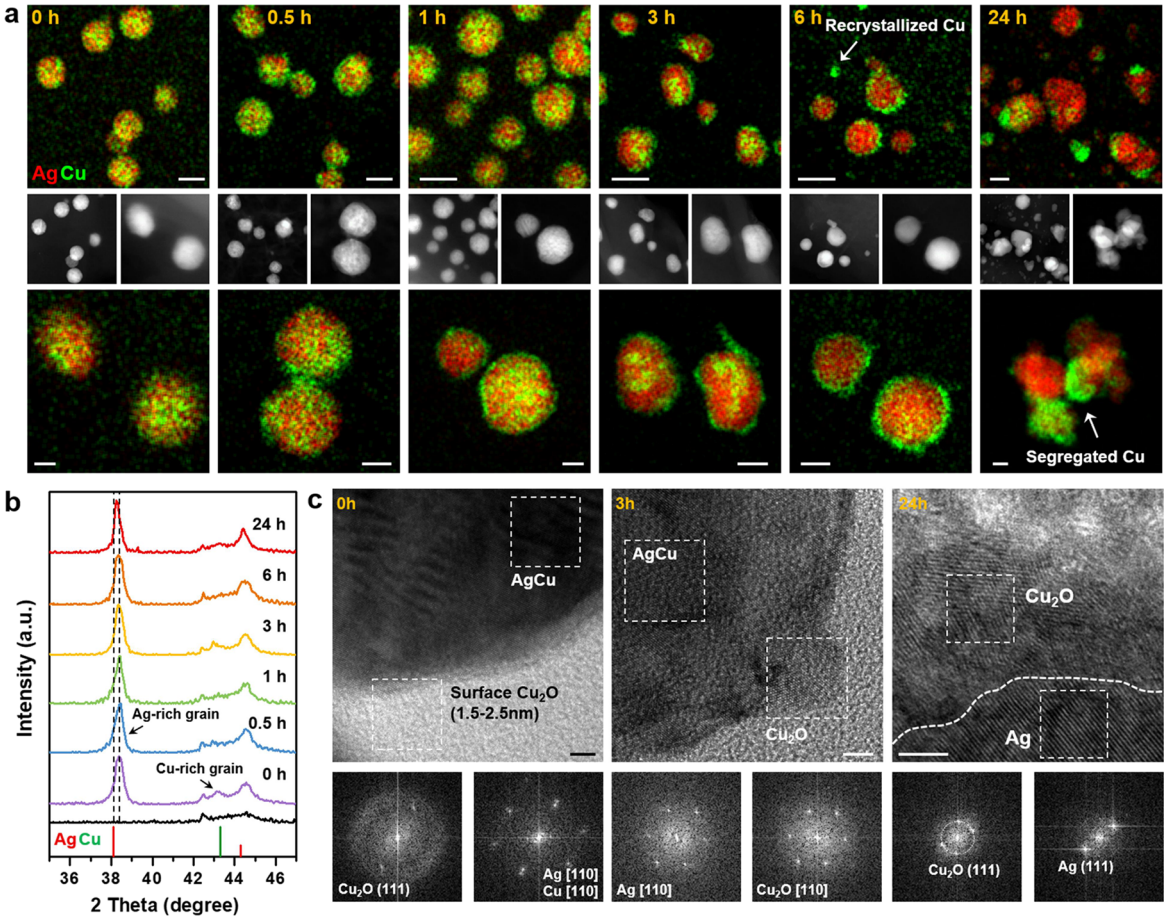

Figure 3. Structural evolution of intermixed AgCu catalysts in CO_2RR. (a) HAADF-STEM images and EDS elemental mapping of I-AgCu catalysts after being used for 0, 0.5, 1, 3, 6, and 24 h of CO_2RR. Scale bars in the top row, 50 nm; bottom row, 20 nm. (b) XRD patterns of I-AgCu particles after catalyzing CO_2RR for a specific time. The black line is the XRD curve of carbon substrates. (c) HRTEM images of I-AgCu catalysts after being used for 0, 3, and 24 h of CO_2RR. The white dashed squares highlight the regions used for FFT analysis. Scale bars, 3 nm.

solubility of Cu species in the electrolyte (0.1 M $KHCO_3$),[46,57] the decreased Cu content cannot be explained by the dissolution of Cu into the electrolyte. We hypothesize that this part of Cu migrates from the catalyst surface to the carbon substrate during the electrolysis, which then agglomerates to form those isolated Cu-rich particles (Figures 3a and S7).

To further verify whether the two unique phases we identified in the AgCu catalysts, i.e., $Ag_{0.88}Cu_{0.12}$ and $Ag_{0.05}Cu_{0.95}$, are thermodynamic products, we utilized thermal treatment to transform I-AgCu catalysts into phase-separated structures (dimeric AgCu, named as D-AgCu), which are supposed to be thermodynamically stable (Figures 5 and S11). Notably, the composition of Cu and Ag domains in the D-AgCu is found to be close to what we have observed in the I-AgCu catalysts after 3 h of CO_2RR. When these D-AgCu catalysts were applied for 3 h of CO_2RR, the Cu domains in the D-AgCu particles are corroded and migrate to the Ag domain surface, resulting in structures similar to the I-AgCu case (Figures 5a and S12). The composition of Ag and Cu domains measured by EDS remains unchanged after the electrolysis (Figures 5b and S11). Besides, there is a negligible peak shift of the Ag(111) and Cu(111) planes in the XRD patterns of the catalysts before and after electrolysis (Figure 5c). As such, we conclude that $Ag_{0.88}Cu_{0.12}$ and $Ag_{0.05}Cu_{0.95}$ are thermodynamic phases in AgCu NPs, which are also stable under the CO_2RR environment.

The structural and compositional studies of the intermixed and phase-separated AgCu NPs clearly point out the separation between Ag and Cu in catalysts during CO_2RR. Since electrocatalysis indeed occurs at the catalyst−electrolyte interface, the surface structure rather than the bulk dictates the catalytic results, of which the importance cannot be ignored. Recently, many analytical techniques have been built up to advance our understanding of the surface chemistry in electrocatalysis.[58,59] Among the various surface characterization technologies, electrochemical methods exhibit their unique advantage by directly acting on the electrode surface and therefore are sensitive to the local chemical environment. For example, H-underpotential deposition has become a classical method to probe the surface area and active sites of Pt-based catalysts,[60] and the redox peak of Ir can be a method to quantify the Ir sites in oxygen evolution catalysts.[44] However, the electrochemical characterization of Cu surfaces is more challenging for various reasons. Although double-layer capacitance can be used to quantify the electrochemical surface area of a Cu foil or mesh, it is not applicable for the carbon-supported Cu NPs due to the large capacitance contributed from the substrates. Meanwhile, the dynamic nature of Cu atoms during the redox cycles often makes surface characterization ambiguous because of the possible severe surface and even bulk structural change. In view of this, researchers have used OH^- adsorption peaks to identify the Cu surface

https://doi.org/10.1021/jacs.3c00467
J. Am. Chem. Soc. 2023, 145, 10116−10125

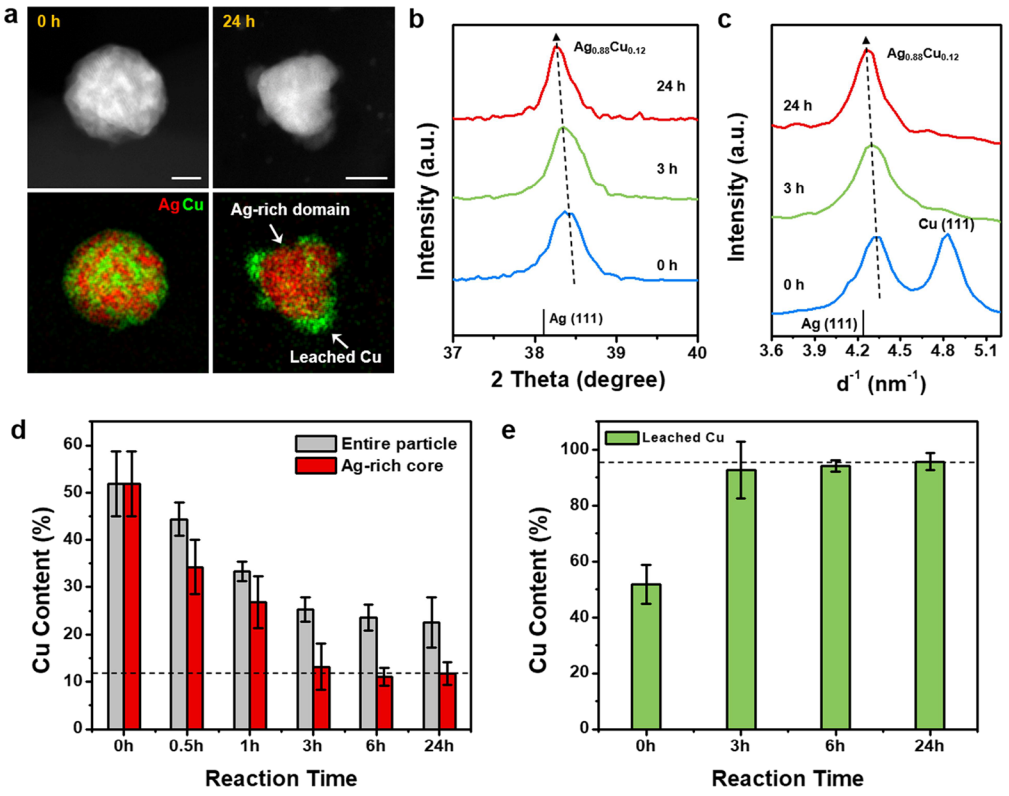

Figure 4. Compositional evolution of intermixed AgCu catalysts in CO_2RR. (a) HAADF-STEM images and EDS elemental mapping of an as-synthesized I-AgCu particle and a particle after catalyzing CO_2RR for 24 h. Scale bars, 20 nm. (b) XRD patterns showing the change in the d-spacing of catalyst (111) planes during CO_2RR. (c) SAED radial intensity profiles of the regions near (111) diffraction, which show the change in the d-spacing of catalyst (111) planes during CO_2RR. (d) Compositional variation of the entire AgCu particles and the Ag-rich core of the catalysts during CO_2RR. (e) Compositional change of the leached Cu species during CO_2RR.

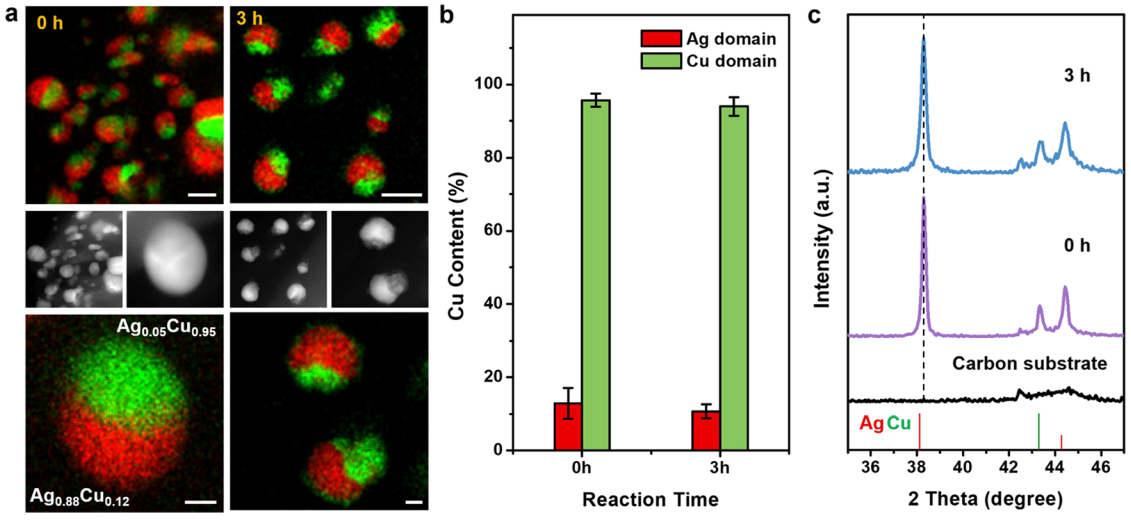

Figure 5. Compositional evolution of phase-separated AgCu catalysts in CO_2RR. (a) HAADF-STEM images and EDS elemental mapping of the as-synthesized D-AgCu particles and particles after catalyzing CO_2RR for 3 h. Scale bars in the top row, 50 nm; bottom row, 10 nm. (b) Compositional change of the Ag and Cu domains in the D-AgCu catalysts during CO_2RR. (c) XRD patterns of the D-AgCu catalysts and the catalysts used for 3 h of CO_2RR.

structure,[61] but these characteristic peaks are also partially overlapped with the Cu oxidation peak, making it challenging to determine the sweeping potential window and analyze the corresponding results.

Recently, Pb underpotential deposition (Pb-UPD) has been utilized to characterize the Cu surface, which is sensitive to the surface structure and has a high signal-to-noise ratio since there is no contribution from the carbon substrates.[62,63] Therefore, we investigated the surface structure of AgCu catalysts with this method (Figures 6 and S13). Commercial Cu and Ag foils were utilized as references, which exhibit Pb stripping peaks at −0.254 and −0.284 V vs Ag/AgCl (3 M KCl), respectively (Figure 6a). Interestingly, in stark difference from the reference, a major stripping peak located at −0.303 V and a

https://doi.org/10.1021/jacs.3c00467
J. Am. Chem. Soc. 2023, 145, 10116−10125

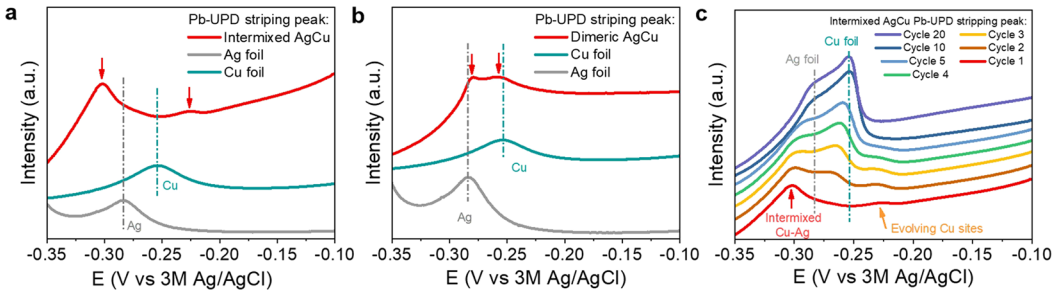

Figure 6. Pb-UPD analysis of intermixed and phase-separated AgCu catalysts. (a) Pb stripping peaks of the I-AgCu particles in Pb-UPD measurements. The first cycle was plotted here to analyze the pristine surface before surface reconstruction. Pb stripping peaks of Cu and Ag foils were included for comparison. (b) Pb stripping peaks of the D-AgCu particles in Pb-UPD experiments. The first cycle was plotted here to avoid any surface reconstruction of the AgCu heterodimers. Pb stripping peaks of Cu and Ag foils were included for comparison. (c) Sequential Pb stripping peaks of the I-AgCu in Pb-UPD experiments. In the Pb-UPD experiments, Pb was deposited on I-AgCu during the cathodic scan and stripped in the anodic scan. 20 CV cycles were recorded to track the surface evolution of the I-AgCu.

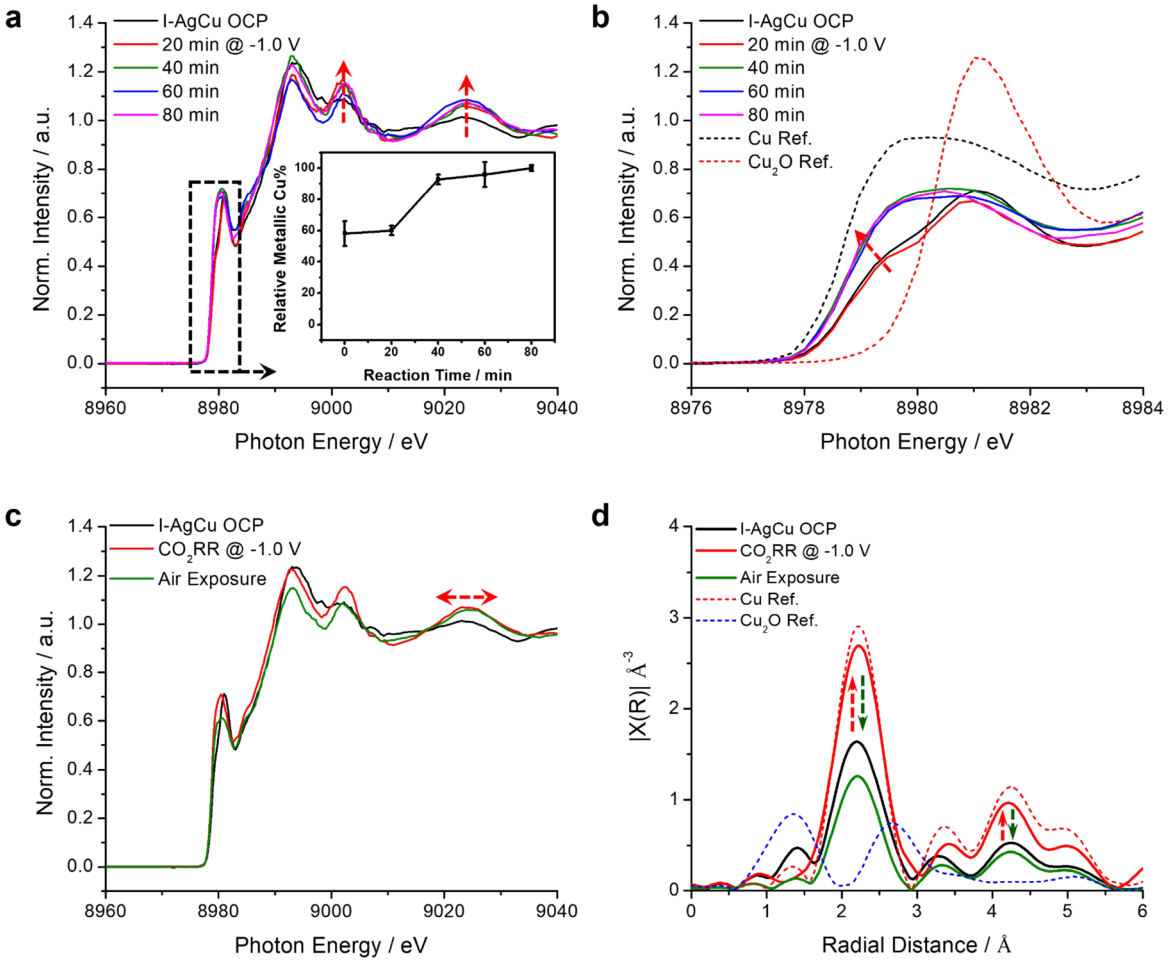

Figure 7. Operando HERFD XAS studies of valence states and coordination environments of intermixed AgCu catalysts during CO_2RR. (a) Operando HERFD XANES of Cu K-edge of the I-AgCu as a function of the reaction time at −1.0 V vs RHE in CO_2-saturated 0.1 M $KHCO_3$. The inset shows the quantitative analysis of the relative metallic Cu fraction. (b) XANES pre-edges of I-AgCu magnified from the dashed box region in (a) and the comparison with Cu and Cu_2O references (dashed lines). (c, d) Operando XANES and the corresponding EXAFS spectra of I-AgCu before, during, and upon air exposure after the CO_2RR.

minor stripping peak located at −0.226 V can be found in the first cyclic voltammetry (CV) cycle of the I-AgCu particles, which may be attributed to the Pb stripping from the intermixed phases and the defected Cu sites,[62] respectively. The minor peak belonging to the defected Cu (−0.226 V) becomes larger in the initial few CV cycles and then vanishes, which can be correlated to Cu leaching, migration, and aggregation. In addition, unlike the Cu and Ag foils, which are stable under the Pb-UPD condition, the Pb stripping peaks of the I-AgCu particles evolve quickly (Figure 6c). It can be seen that the pristine −0.303 V peak gradually decreases and separates into two peaks that match well with the peak positions of the Cu and Ag foils. This indicates that during the electrochemical CO_2RR, the surface of the I-AgCu also

https://doi.org/10.1021/jacs.3c00467
J. Am. Chem. Soc. 2023, 145, 10116−10125

experiences phase separation, resulting in Cu- and Ag-dominated phases. Since the Pb stripping peak only reflects the binding strength between the metal surface and Pb atoms, it is arguable whether the surface comprises pure Cu and Ag phases or the trace inter-doping of metals does not significantly influence the Pb-binding affinity. However, considering that the inter-doped phases in the D-AgCu particles exhibit a shift of Pb stripping peaks (Figure 6b), we believe there is no inter-doping between Cu and Ag on the particle surface after the phase separation caused by CO_2RR. Collectively, Pb-UPD experiments confirm that the AgCu mixture is not stable under CO_2RR conditions. Not only the bulk but also the surface of AgCu catalysts goes through an electrochemically triggered phase separation. The results also imply that the enhanced CO_2RR performance reported on AgCu catalysts could be originated from AgCu heterostructures. Such structures can promote CO_2RR tandem catalysis between the Ag and Cu domains as well as boost CO_2RR via the asymmetric coupling sites that are rich around the AgCu interface. Therefore, constructing phase boundary-rich AgCu catalysts will be beneficial for enhanced CO_2RR.

In addition to investigate the structural fate of AgCu catalysts, we further employed operando high-energy-resolution fluorescence detected (HERFD) XAS to unravel the chemical state of the catalysts during CO_2RR, i.e., the electronic structure and coordination environment of I-AgCu electrocatalysts under real-time reaction conditions. The HERFD detector selects the Cu $K\alpha_1$ emission line as one particular fluorescence decay channel, which significantly extends the core hole lifetime.[64,65] Thus, HERFD XAS can allow a much higher energy resolution on the order of 1 eV, given the energy−time uncertainty principle, when compared to a conventional X-ray fluorescence detector (50−200 eV).[49,66,67] HERFD X-ray absorption near-edge structure (XANES) spectroscopy resolves the pre-edge peaks of Cu, Cu_2O, and CuO reference samples, which are significantly better than conventional XANES spectra, as exemplified by the notable identification of the pre-peak of CuO at ∼8977 eV originating from the Jahn−Teller distortion of the $[Ar]3d^9$ configuration (Figure S14). Cu_2O shows the characteristic pre-edge peak at 8981.0 eV with a 1.2 eV positive shift, relative to Cu (8979.8 eV). The home-made HERFD XAS electrochemical cell[68] is capable of delivering electrochemical results of I-AgCu electrocatalysts comparable to a standard H-cell with a well-defined current plateau under the CO_2RR condition (Figure S15).

Operando XANES of I-AgCu electrocatalysts was performed during the CO_2RR (Figure 7a). The XANES spectrum of pristine I-AgCu presents the co-existence of metallic Cu and Cu_2O when compared to standard references (Figure 7b, dashed lines). At −1.0 V vs RHE, XANES pre-edge peaks at ∼8979 eV show progressive negative shifts, particularly after 40 min, corresponding to the electroreduction of Cu_2O to metallic Cu. In addition, post-edge peaks at 9002.5 and 9024 eV (dashed red arrows in Figure 7a) further support the conversion of Cu_2O to Cu under the reaction environment (Figure S14b). Quantitative analysis using pre-edge peaks suggests that the metallic Cu fraction increases from about 60% of the pristine I-AgCu to about 90% after 40 min and approaches 100% after 80 min of electroreduction (Figures 7a and S16). The corresponding extended X-ray absorption fine structure (EXAFS) spectra show the diminution of Cu−O bonding and the increasing contributions of Cu−Cu bonding (Figures 7d and S17). The operando X-ray studies suggest that metallic Cu is the active state in AgCu for catalyzing CO_2RR.

One pressing challenge facing the development of Cu electrocatalysts is whether the re-oxidation (i.e., deactivation) of active metallic Cu sites can be mitigated so as to maintain active structures after the CO_2RR and enhance the catalyst durability in realistic applications.[49,69,70] After three-week air exposure, we examined the ex situ XAS of AgCu electrocatalysts (Figure 7c,d). Surprisingly, the evolved AgCu catalysts exhibit a significant fraction of metallic Cu, as indicated by the horizontal dashed line in XANES spectra (Figure 7c). k^2-Weighted EXAFS spectra clearly show that AgCu electrocatalysts experience electroreduction from Cu_2O to metallic Cu during CO_2RR (red dashed arrows) (Figure 7d). Upon long-time air exposure, Cu in the evolved AgCu catalysts mainly maintains the metallic feature, as evidenced by the lack of Cu−O bonding at 1.5 Å and the persistent existence of triplet metallic Cu features at ∼4.5 Å (note that no phase correction was applied to EXAFS analysis). The amplitude of Cu−Cu bonding exhibits a noticeable decay upon air exposure (green dashed arrows), which is possibly due to the structural reconstruction, such as fracturing of large Cu domains, leading to lower coordination numbers and/or more disordered structures upon air exposure. Collectively, operando HERFD XANES and EXAFS present clear evidence to show that Cu in the AgCu catalysts is fully reduced to metallic Cu as possible active sites for the CO_2RR, and Ag in the evolved AgCu catalysts is instrumental in suppressing Cu oxidation upon air exposure. In our previous study on the Cu NP ensemble,[49] during CO_2RR, sub-10 nm (7 nm) Cu NPs evolved into metallic Cu nanograins, which were fully oxidized to Cu_2O cubes upon air exposure, while 18 nm NP-derived Cu nanograins were transformed to Cu@Cu_2O core−shell particles when exposed to air. In comparison, it is surprising that Cu_2O cubes were not observed in the AgCu system, even for those small-size leached Cu species. This is possibly attributable to the suppressed Cu-oxidation effect induced by Ag, as demonstrated by the EXAFS measurements (Figure 7c,d). In addition, the average size of the original AgCu particles is around 60 nm (Figure S8), making their oxidation behavior more similar to those larger Cu catalysts, i.e., forming a surface Cu_2O layer upon air exposure rather than recrystallizing into Cu_2O cubes.

CONCLUSIONS

In summary, we have systematically explored the structural and chemical evolution of intermixed and phase-separated AgCu catalysts under electrochemical CO_2RR conditions. Cu exhibits high mobility during CO_2RR, which can migrate to the catalyst surface, detach from the catalysts, and recrystallize as new particles. Meanwhile, the poor compatibility between Ag and Cu triggers their separation in spite of their initial mixing state. Eventually, the catalysts will evolve into structures composed of two phases, i.e., $Ag_{0.88}Cu_{0.12}$ and $Ag_{0.05}Cu_{0.95}$, that are thermodynamically stable under CO_2RR conditions. This separation phenomenon not only occurs in the bulk of the catalysts but also on the catalyst surface, suggesting that AgCu heterostructures account for the enhanced CO_2RR in AgCu catalysts. In terms of the valence state, our operando XAS study confirms the Cu(0) state in the AgCu catalysts during the reaction as well as the enhanced anti-oxidation of the evolved AgCu catalysts, as compared with Cu catalysts. Our work unveils how AgCu bimetallic catalysts structurally and

https://doi.org/10.1021/jacs.3c00467
J. Am. Chem. Soc. 2023, 145, 10116−10125

chemically evolve during CO_2RR, which not only advances the understanding of the interaction between Cu and Ag but also sheds light on the active AgCu structures for CO_2RR and provides insights into the design of efficient AgCu catalysts for CO_2RR.

■ ASSOCIATED CONTENT

Supporting Information

The Supporting Information is available free of charge at https://pubs.acs.org/doi/10.1021/jacs.3c00467.

EDS analysis of I-AgCu and D-AgCu catalysts, HRTEM images of I-AgCu catalysts after CO_2RR, SAED analysis of I-AgCu catalysts after CO_2RR, CO_2RR performance of I-AgCu and pure Cu catalysts, CV curves of Pb-UPD, and XAS analysis of I-AgCu catalysts (PDF)

■ AUTHOR INFORMATION

Corresponding Author

Peidong Yang − *Kavli Energy Nanoscience Institute, Department of Chemistry, and Department of Materials Science and Engineering, University of California, Berkeley, California 94720, United States;* orcid.org/0000-0003-4799-1684; Email: p_yang@berkeley.edu

Authors

Peng-Cheng Chen − *Kavli Energy Nanoscience Institute and Department of Chemistry, University of California, Berkeley, California 94720, United States;* Present Address: Department of Materials Science, Fudan University, Shanghai 200438, China; orcid.org/0000-0002-0411-9549

Chubai Chen − *Department of Chemistry, University of California, Berkeley, California 94720, United States;* orcid.org/0000-0003-2513-2707

Yao Yang − *Department of Chemistry and Miller Institute, University of California, Berkeley, California 94720, United States*

Arifin Luthfi Maulana − *Department of Materials Science and Engineering, University of California, Berkeley, California 94720, United States*

Jianbo Jin − *Department of Chemistry, University of California, Berkeley, California 94720, United States;* orcid.org/0000-0002-9054-7960

Julian Feijoo − *Department of Chemistry, University of California, Berkeley, California 94720, United States*

Complete contact information is available at: https://pubs.acs.org/10.1021/jacs.3c00467

Author Contributions

#P.-C.C., C.C., and Y.Y. contributed equally to this work.

Notes

The authors declare no competing financial interest.

■ ACKNOWLEDGMENTS

This work was supported by the Director, Office of Science, Office of Basic Energy Sciences, Chemical Sciences, Geosciences, and Biosciences Division of the U.S. Department of Energy under Contract No. DE-AC02-05CH11231, FWP CH030201 (Catalysis Research Program). Work at the Molecular Foundry was supported by the Office of Science, Office of Basic Energy Sciences of the U.S. Department of Energy under Contract No. DE-AC02-05CH11231. This work is based on research conducted at the Center for High-Energy X-ray Sciences (CHEXS), which is supported by the National Science Foundation (BIO, ENG and MPS Directorates) under award DMR-1829070. P.-C.C. acknowledges support from Kavli ENSI Heising-Simons Fellowship. C.C. and J.J. acknowledge fellowship support from Suzhou Industrial Park. Y.Y. acknowledges support from Miller Fellowship. We thank Dr. Christopher Pollock at CHESS PIPOXS beamlines for the HERFD XAS setup.

■ REFERENCES

(1) Bushuyev, O. S.; De Luna, P.; Dinh, C. T.; Tao, L.; Saur, G.; van de Lagemaat, J.; Kelley, S. O.; Sargent, E. H. What Should We Make with CO_2 and How Can We Make It? *Joule* **2018**, *2*, 825−832.

(2) Hepburn, C.; Adlen, E.; Beddington, J.; Carter, E. A.; Fuss, S.; Mac Dowell, N.; Minx, J. C.; Smith, P.; Williams, C. K. The technological and economic prospects for CO_2 utilization and removal. *Nature* **2019**, *575*, 87−97.

(3) Ross, M. B.; De Luna, P.; Li, Y.; Dinh, C.-T.; Kim, D.; Yang, P.; Sargent, E. H. Designing materials for electrochemical carbon dioxide recycling. *Nat. Catal.* **2019**, *2*, 648−658.

(4) Varela, A. S.; Ju, W.; Bagger, A.; Franco, P.; Rossmeisl, J.; Strasser, P. Electrochemical Reduction of CO2 on Metal-Nitrogen-Doped Carbon Catalysts. *ACS Catal.* **2019**, *9*, 7270−7284.

(5) Birdja, Y. Y.; Pérez-Gallent, E.; Figueiredo, M. C.; Göttle, A. J.; Calle-Vallejo, F.; Koper, M. T. M. Advances and challenges in understanding the electrocatalytic conversion of carbon dioxide to fuels. *Nat. Energy* **2019**, *4*, 732−745.

(6) Nitopi, S.; Bertheussen, E.; Scott, S. B.; Liu, X.; Engstfeld, A. K.; Horch, S.; Seger, B.; Stephens, I. E. L.; Chan, K.; Hahn, C.; Nørskov, J. K.; Jaramillo, T. F.; Chorkendorff, I. Progress and Perspectives of Electrochemical CO_2 Reduction on Copper in Aqueous Electrolyte. *Chem. Rev.* **2019**, *119*, 7610−7672.

(7) Lee, C. W.; Yang, K. D.; Nam, D.-H.; Jang, J. H.; Cho, N. H.; Im, S. W.; Nam, K. T. Defining a Materials Database for the Design of Copper Binary Alloy Catalysts for Electrochemical CO_2 Conversion. *Adv. Mater.* **2018**, *30*, No. 1704717.

(8) Bagger, A.; Ju, W.; Varela, A. S.; Strasser, P.; Rossmeisl, J. Electrochemical CO_2 Reduction: A Classification Problem. *ChemPhysChem* **2017**, *18*, 3266−3273.

(9) Liu, K.; Ma, M.; Wu, L.; Valenti, M.; Cardenas-Morcoso, D.; Hofmann, J. P.; Bisquert, J.; Gimenez, S.; Smith, W. A. Electronic Effects Determine the Selectivity of Planar Au−Cu Bimetallic Thin Films for Electrochemical CO2 Reduction. *ACS Appl. Mater. Interfaces* **2019**, *11*, 16546−16555.

(10) Nellaiappan, S.; Katiyar, N. K.; Kumar, R.; Parui, A.; Malviya, K. D.; Pradeep, K. G.; Singh, A. K.; Sharma, S.; Tiwary, C. S.; Biswas, K. High-Entropy Alloys as Catalysts for the CO_2 and CO Reduction Reactions: Experimental Realization. *ACS Catal.* **2020**, *10*, 3658−3663.

(11) Morales-Guio, C. G.; Cave, E. R.; Nitopi, S. A.; Feaster, J. T.; Wang, L.; Kuhl, K. P.; Jackson, A.; Johnson, N. C.; Abram, D. N.; Hatsukade, T.; Hahn, C.; Jaramillo, T. F. Improved CO2 reduction activity towards C2+ alcohols on a tandem gold on copper electrocatalyst. *Nat. Catal.* **2018**, *1*, 764−771.

(12) Zhang, H.; Chang, X.; Chen, J. G.; Goddard, W. A.; Xu, B.; Cheng, M.-J.; Lu, Q. Computational and experimental demonstrations of one-pot tandem catalysis for electrochemical carbon dioxide reduction to methane. *Nat. Commun.* **2019**, *10*, 3340.

(13) Kim, D.; Resasco, J.; Yu, Y.; Asiri, A. M.; Yang, P. Synergistic geometric and electronic effects for electrochemical reduction of carbon dioxide using gold−copper bimetallic nanoparticles. *Nat. Commun.* **2014**, *5*, 4948.

(14) Clark, E. L.; Hahn, C.; Jaramillo, T. F.; Bell, A. T. Electrochemical CO_2 Reduction over Compressively Strained CuAg Surface Alloys with Enhanced Multi-Carbon Oxygenate Selectivity. *J. Am. Chem. Soc.* **2017**, *139*, 15848−15857.

(15) Chang, C.-J.; Lin, S.-C.; Chen, H.-C.; Wang, J.; Zheng, K. J.; Zhu, Y.; Chen, H. M. Dynamic Reoxidation/Reduction-Driven Atomic Interdiffusion for Highly Selective CO_2 Reduction toward Methane. *J. Am. Chem. Soc.* **2020**, *142*, 12119−12132.
(16) Li, Y. C.; Wang, Z.; Yuan, T.; Nam, D.-H.; Luo, M.; Wicks, J.; Chen, B.; Li, J.; Li, F.; de Arquer, F. P. G.; Wang, Y.; Dinh, C.-T.; Voznyy, O.; Sinton, D.; Sargent, E. H. Binding Site Diversity Promotes CO2 Electroreduction to Ethanol. *J. Am. Chem. Soc.* **2019**, *141*, 8584−8591.
(17) Gurudayal; Perone, D.; Malani, S.; Lum, Y.; Haussener, S.; Ager, J. W. Sequential Cascade Electrocatalytic Conversion of Carbon Dioxide to C−C Coupled Products. *ACS Appl. Energy Mater.* **2019**, *2*, 4551−4559.
(18) Lum, Y.; Ager, J. W. Sequential catalysis controls selectivity in electrochemical CO2 reduction on Cu. *Energy Environ. Sci.* **2018**, *11*, 2935−2944.
(19) Chen, C.; Li, Y.; Yu, S.; Louisia, S.; Jin, J.; Li, M.; Ross, M. B.; Yang, P. Cu-Ag Tandem Catalysts for High-Rate CO2 Electrolysis toward Multicarbons. *Joule* **2020**, *4*, 1688−1699.
(20) Xie, Y.; Ou, P.; Wang, X.; Xu, Z.; Li, Y. C.; Wang, Z.; Huang, J. E.; Wicks, J.; McCallum, C.; Wang, N.; Wang, Y.; Chen, T.; Lo, B. T. W.; Sinton, D.; Yu, J. C.; Wang, Y.; Sargent, E. H. High carbon utilization in CO_2 reduction to multi-carbon products in acidic media. *Nat. Catal.* **2022**, *5*, 564−570.
(21) Lyu, Z.; Zhu, S.; Xu, L.; Chen, Z.; Zhang, Y.; Xie, M.; Li, T.; Zhou, S.; Liu, J.; Chi, M.; Shao, M.; Mavrikakis, M.; Xia, Y. Kinetically Controlled Synthesis of Pd−Cu Janus Nanocrystals with Enriched Surface Structures and Enhanced Catalytic Activities toward CO_2 Reduction. *J. Am. Chem. Soc.* **2021**, *143*, 149−162.
(22) Merino-Garcia, I.; Albo, J.; Krzywda, P.; Mul, G.; Irabien, A. Bimetallic Cu-based hollow fibre electrodes for CO_2 electroreduction. *Catal. Today* **2020**, *346*, 34−39.
(23) Albo, J.; Sáez, A.; Solla-Gullón, J.; Montiel, V.; Irabien, A. Production of methanol from CO_2 electroreduction at Cu_2O and Cu_2O/ZnO-based electrodes in aqueous solution. *Appl. Catal., B* **2015**, *176*, 709−717.
(24) Merino-Garcia, I.; Albo, J.; Solla-Gullón, J.; Montiel, V.; Irabien, A. Cu oxide/ZnO-based surfaces for a selective ethylene production from gas-phase CO_2 electroconversion. *J. CO2 Util.* **2019**, *31*, 135−142.
(25) Albo, J.; Vallejo, D.; Beobide, G.; Castillo, O.; Castaño, P.; Irabien, A. Copper-Based Metal−Organic Porous Materials for CO2 Electrocatalytic Reduction to Alcohols. *ChemSusChem* **2017**, *10*, 1100−1109.
(26) Zhong, M.; Tran, K.; Min, Y.; Wang, C.; Wang, Z.; Dinh, C.-T.; De Luna, P.; Yu, Z.; Rasouli, A. S.; Brodersen, P.; Sun, S.; Voznyy, O.; Tan, C.-S.; Askerka, M.; Che, F.; Liu, M.; Seifitokaldani, A.; Pang, Y.; Lo, S.-C.; Ip, A.; Ulissi, Z.; Sargent, E. H. Accelerated discovery of CO_2 electrocatalysts using active machine learning. *Nature* **2020**, *581*, 178−183.
(27) Kim, D.; Yu, S.; Zheng, F.; Roh, I.; Li, Y.; Louisia, S.; Qi, Z.; Somorjai, G. A.; Frei, H.; Wang, L.-W.; Yang, P. Selective CO_2 electrocatalysis at the pseudocapacitive nanoparticle/ordered-ligand interlayer. *Nat. Energy* **2020**, *5*, 1032−1042.
(28) Bui, J. C.; Kim, C.; King, A. J.; Romiluyi, O.; Kusoglu, A.; Weber, A. Z.; Bell, A. T. Engineering Catalyst−Electrolyte Microenvironments to Optimize the Activity and Selectivity for the Electrochemical Reduction of CO_2 on Cu and Ag. *Acc. Chem. Res.* **2022**, *55*, 484−494.
(29) *Alloy Phase Diagrams. ASM Handbook*; Okamoto, H.; Schlesinger, M. E.; Mueller, E. M., Eds.; ASM International: Materials Park, OH, 2016; vol 3.
(30) Chen, P. C.; Liu, X. L.; Hedrick, J. L.; Xie, Z.; Wang, S. Z.; Lin, Q. Y.; Hersam, M. C.; Dravid, V. P.; Mirkin, C. A. Polyelemental nanoparticle libraries. *Science* **2016**, *352*, 1565−1569.
(31) Chen, P. C.; Du, J. S. S.; Meckes, B.; Huang, L. L.; Xie, Z.; Hedrick, J. L.; Dravid, V. P.; Mirkin, C. A. Structural Evolution of Three-Component Nanoparticles in Polymer Nanoreactors. *J. Am. Chem. Soc.* **2017**, *139*, 9876−9884.
(32) Chen, P. C.; Liu, M. H.; Du, J. S. S.; Meckes, B.; Wang, S. Z.; Lin, H. X.; Dravid, V. P.; Wolverton, C.; Mirkin, C. A. Interface and heterostructure design in polyelemental nanoparticles. *Science* **2019**, *363*, 959−964.
(33) Chen, C.; Yu, S.; Yang, Y.; Louisia, S.; Roh, I.; Jin, J.; Chen, S.; Chen, P.-C.; Shan, Y.; Yang, P. Exploration of the bio-analogous asymmetric C−C coupling mechanism in tandem CO_2 electroreduction. *Nat. Catal.* **2022**, *5*, 878−887.
(34) Dutta, A.; Montiel, I. Z.; Erni, R.; Kiran, K.; Rahaman, M.; Drnec, J.; Broekmann, P. Activation of bimetallic AgCu foam electrocatalysts for ethanol formation from CO_2 by selective Cu oxidation/reduction. *Nano Energy* **2020**, *68*, No. 104331.
(35) Huang, J.; Mensi, M.; Oveisi, E.; Mantella, V.; Buonsanti, R. Structural Sensitivities in Bimetallic Catalysts for Electrochemical CO_2 Reduction Revealed by Ag−Cu Nanodimers. *J. Am. Chem. Soc.* **2019**, *141*, 2490−2499.
(36) O'Mara, P. B.; Wilde, P.; Benedetti, T. M.; Andronescu, C.; Cheong, S.; Gooding, J. J.; Tilley, R. D.; Schuhmann, W. Cascade Reactions in Nanozymes: Spatially Separated Active Sites inside Ag-Core−Porous-Cu-Shell Nanoparticles for Multistep Carbon Dioxide Reduction to Higher Organic Molecules. *J. Am. Chem. Soc.* **2019**, *141*, 14093−14097.
(37) Lee, S.; Park, G.; Lee, J. Importance of Ag−Cu Biphasic Boundaries for Selective Electrochemical Reduction of CO2 to Ethanol. *ACS Catal.* **2017**, *7*, 8594−8604.
(38) Ting, L. R. L.; Piqué, O.; Lim, S. Y.; Tanhaei, M.; Calle-Vallejo, F.; Yeo, B. S. Enhancing CO_2 Electroreduction to Ethanol on Copper−Silver Composites by Opening an Alternative Catalytic Pathway. *ACS Catal.* **2020**, *10*, 4059−4069.
(39) Gao, J.; Zhang, H.; Guo, X.; Luo, J.; Zakeeruddin, S. M.; Ren, D.; Grätzel, M. Selective C−C Coupling in Carbon Dioxide Electroreduction via Efficient Spillover of Intermediates As Supported by Operando Raman Spectroscopy. *J. Am. Chem. Soc.* **2019**, *141*, 18704−18714.
(40) Chen, P.-C.; Gao, M.; Yu, S.; Jin, J.; Song, C.; Salmeron, M.; Scott, M. C.; Yang, P. Revealing the Phase Separation Behavior of Thermodynamically Immiscible Elements in a Nanoparticle. *Nano Lett.* **2021**, *21*, 6684−6689.
(41) Wang, X.; Wang, Z.; Zhuang, T.-T.; Dinh, C.-T.; Li, J.; Nam, D.-H.; Li, F.; Huang, C.-W.; Tan, C.-S.; Chen, Z.; Chi, M.; Gabardo, C. M.; Seifitokaldani, A.; Todorović, P.; Proppe, A.; Pang, Y.; Kirmani, A. R.; Wang, Y.; Ip, A. H.; Richter, L. J.; Scheffel, B.; Xu, A.; Lo, S.-C.; Kelley, S. O.; Sinton, D.; Sargent, E. H. Efficient upgrading of CO to C3 fuel using asymmetric C-C coupling active sites. *Nat. Commun.* **2019**, *10*, 5186.
(42) Hoang, T. T. H.; Verma, S.; Ma, S.; Fister, T. T.; Timoshenko, J.; Frenkel, A. I.; Kenis, P. J. A.; Gewirth, A. A. Nanoporous Copper−Silver Alloys by Additive-Controlled Electrodeposition for the Selective Electroreduction of CO2 to Ethylene and Ethanol. *J. Am. Chem. Soc.* **2018**, *140*, 5791−5797.
(43) Yang, C.; Ko, B. H.; Hwang, S.; Liu, Z.; Yao, Y.; Luc, W.; Cui, M.; Malkani, A. S.; Li, T.; Wang, X.; Dai, J.; Xu, B.; Wang, G.; Su, D.; Jiao, F.; Hu, L. Overcoming immiscibility toward bimetallic catalyst library. *Sci. Adv.* **2020**, *6*, No. eaaz6844.
(44) Chen, P.-C.; Li, M.; Jin, J.; Yu, S.; Chen, S.; Chen, C.; Salmeron, M.; Yang, P. Heterostructured Au−Ir Catalysts for Enhanced Oxygen Evolution Reaction. *ACS Mater. Lett.* **2021**, *3*, 1440−1447.
(45) Wilde, P.; O'Mara, P. B.; Junqueira, J. R. C.; Tarnev, T.; Benedetti, T. M.; Andronescu, C.; Chen, Y.-T.; Tilley, R. D.; Schuhmann, W.; Gooding, J. J. Is Cu instability during the CO2 reduction reaction governed by the applied potential or the local CO concentration? *Chem. Sci.* **2021**, *12*, 4028−4033.
(46) Huang, J.; Hörmann, N.; Oveisi, E.; Loiudice, A.; De Gregorio, G. L.; Andreussi, O.; Marzari, N.; Buonsanti, R. Potential-induced nanoclustering of metallic catalysts during electrochemical CO2 reduction. *Nat. Commun.* **2018**, *9*, 3117.
(47) Wang, H.; Zhou, X.; Yu, T.; Lu, X.; Qian, L.; Liu, P.; Lei, P. Surface restructuring in AgCu single-atom alloy catalyst and self-

enhanced selectivity toward CO_2 reduction. *Electrochim. Acta* **2022**, *426*, No. 140774.
(48) Popović, S.; Smiljanić, M.; Jovanovič, P.; Vavra, J.; Buonsanti, R.; Hodnik, N. Stability and Degradation Mechanisms of Copper-Based Catalysts for Electrochemical CO_2 Reduction. *Angew. Chem., Int. Ed.* **2020**, *59*, 14736−14746.
(49) Yang, Y.; Louisia, S.; Yu, S.; Jin, J.; Roh, I.; Chen, C.; Fonseca Guzman, M. V.; Feijoo, J.; Chen, P.-C.; Wang, H.; Pollock, C. J.; Huang, X.; Shao, Y.-T.; Wang, C.; Muller, D. A.; Abruña, H. D.; Yang, P. *Operando* Studies Reveal Active Cu Nanograins for CO_2 Electroreduction. *Nature* **2023**, *614*, 262−269.
(50) Kim, Y.-G.; Javier, A.; Baricuatro, J. H.; Soriaga, M. P. Regulating the Product Distribution of CO Reduction by the Atomic-Level Structural Modification of the Cu Electrode Surface. *Electrocatalysis* **2016**, *7*, 391−399.
(51) Varela, A. S.; Schlaup, C.; Jovanov, Z. P.; Malacrida, P.; Horch, S.; Stephens, I. E. L.; Chorkendorff, I. CO2 Electroreduction on Well-Defined Bimetallic Surfaces: Cu Overlayers on Pt(111) and Pt(211). *J. Phys. Chem. C* **2013**, *117*, 20500−20508.
(52) Simon, G. H.; Kley, C. S.; Roldan Cuenya, B. Potential-Dependent Morphology of Copper Catalysts During CO2 Electroreduction Revealed by In Situ Atomic Force Microscopy. *Angew. Chem., Int. Ed.* **2021**, *60*, 2561−2568.
(53) Fei, H.; Dong, J.; Wan, C.; Zhao, Z.; Xu, X.; Lin, Z.; Wang, Y.; Liu, H.; Zang, K.; Luo, J.; Zhao, S.; Hu, W.; Yan, W.; Shakir, I.; Huang, Y.; Duan, X. Microwave-Assisted Rapid Synthesis of Graphene-Supported Single Atomic Metals. *Adv. Mater.* **2018**, *30*, No. 1802146.
(54) Lee, S. H.; Lin, J. C.; Farmand, M.; Landers, A. T.; Feaster, J. T.; Avilés Acosta, J. E.; Beeman, J. W.; Ye, Y.; Yano, J.; Mehta, A.; Davis, R. C.; Jaramillo, T. F.; Hahn, C.; Drisdell, W. S. Oxidation State and Surface Reconstruction of Cu under CO_2 Reduction Conditions from In Situ X-ray Characterization. *J. Am. Chem. Soc.* **2021**, *143*, 588−592.
(55) Wang, H.; Liang, Z.; Tang, M.; Chen, G.; Li, Y.; Chen, W.; Lin, D.; Zhang, Z.; Zhou, G.; Li, J.; Lu, Z.; Chan, K.; Tan, T.; Cui, Y. Self-Selective Catalyst Synthesis for CO_2 Reduction. *Joule* **2019**, *3*, 1927−1936.
(56) Wang, Y.; Wang, Z.; Dinh, C.-T.; Li, J.; Ozden, A.; Golam Kibria, M.; Seifitokaldani, A.; Tan, C.-S.; Gabardo, C. M.; Luo, M.; Zhou, H.; Li, F.; Lum, Y.; McCallum, C.; Xu, Y.; Liu, M.; Proppe, A.; Johnston, A.; Todorovic, P.; Zhuang, T.-T.; Sinton, D.; Kelley, S. O.; Sargent, E. H. Catalyst synthesis under CO_2 electroreduction favours faceting and promotes renewable fuels electrosynthesis. *Nat. Catal.* **2020**, *3*, 98−106.
(57) Möller, T.; Scholten, F.; Thanh, T. N.; Sinev, I.; Timoshenko, J.; Wang, X.; Jovanov, Z.; Gliech, M.; Roldan Cuenya, B.; Varela, A. S.; Strasser, P. Electrocatalytic CO_2 Reduction on CuOx Nanocubes: Tracking the Evolution of Chemical State, Geometric Structure, and Catalytic Selectivity using Operando Spectroscopy. *Angew. Chem., Int. Ed.* **2020**, *59*, 17974−17983.
(58) Timoshenko, J.; Roldan Cuenya, B. In Situ/Operando Electrocatalyst Characterization by X-ray Absorption Spectroscopy. *Chem. Rev.* **2021**, *121*, 882−961.
(59) Deng, Y.; Handoko, A. D.; Du, Y.; Xi, S.; Yeo, B. S. In Situ Raman Spectroscopy of Copper and Copper Oxide Surfaces during Electrochemical Oxygen Evolution Reaction: Identification of CuIII Oxides as Catalytically Active Species. *ACS Catal.* **2016**, *6*, 2473−2481.
(60) Huang, X.; Zhao, Z.; Cao, L.; Chen, Y.; Zhu, E.; Lin, Z.; Li, M.; Yan, A.; Zettl, A.; Wang, Y. M.; Duan, X.; Mueller, T.; Huang, Y. High-performance transition metal-doped Pt_3Ni octahedra for oxygen reduction reaction. *Science* **2015**, *348*, 1230−1234.
(61) Arán-Ais, R. M.; Scholten, F.; Kunze, S.; Rizo, R.; Roldan Cuenya, B. The role of in situ generated morphological motifs and Cu(i) species in C2+ product selectivity during CO_2 pulsed electroreduction. *Nat. Energy* **2020**, *5*, 317−325.
(62) Li, Y.; Kim, D.; Louisia, S.; Xie, C.; Kong, Q.; Yu, S.; Lin, T.; Aloni, S.; Fakra, S. C.; Yang, P. Electrochemically scrambled nanocrystals are catalytically active for CO_2-to-multicarbons. *Proc. Natl. Acad. Sci. U. S. A.* **2020**, *117*, 9194−9201.
(63) Sebastián-Pascual, P.; Escudero-Escribano, M. Surface characterization of copper electrocatalysts by lead underpotential deposition. *J. Electroanal. Chem.* **2021**, *896*, No. 115446.
(64) Glatzel, P.; Bergmann, U. High resolution 1s core hole X-ray spectroscopy in 3d transition metal complexes—electronic and structural information. *Coord. Chem. Rev.* **2005**, *249*, 65−95.
(65) Walroth, R. C.; Uebler, J. W. H.; Lancaster, K. M. Probing CuI in homogeneous catalysis using high-energy-resolution fluorescence-detected X-ray absorption spectroscopy. *Chem. Commun.* **2015**, *51*, 9864−9867.
(66) Yang, Y.; Xiong, Y.; Zeng, R.; Lu, X.; Krumov, M.; Huang, X.; Xu, W.; Wang, H.; DiSalvo, F. J.; Brock, J. D.; Muller, D. A.; Abruña, H. D. Operando Methods in Electrocatalysis. *ACS Catal.* **2021**, *11*, 1136−1178.
(67) Friebel, D.; Louie, M. W.; Bajdich, M.; Sanwald, K. E.; Cai, Y.; Wise, A. M.; Cheng, M.-J.; Sokaras, D.; Weng, T.-C.; Alonso-Mori, R.; Davis, R. C.; Bargar, J. R.; Nørskov, J. K.; Nilsson, A.; Bell, A. T. Identification of Highly Active Fe Sites in (Ni,Fe)OOH for Electrocatalytic Water Splitting. *J. Am. Chem. Soc.* **2015**, *137*, 1305−1313.
(68) Yang, Y.; Wang, Y.; Xiong, Y.; Huang, X.; Shen, L.; Huang, R.; Wang, H.; Pastore, J. P.; Yu, S.-H.; Xiao, L.; Brock, J. D.; Zhuang, L.; Abruña, H. D. In Situ X-ray Absorption Spectroscopy of a Synergistic Co−Mn Oxide Catalyst for the Oxygen Reduction Reaction. *J. Am. Chem. Soc.* **2019**, *141*, 1463−1466.
(69) Scott, S. B.; Hogg, T. V.; Landers, A. T.; Maagaard, T.; Bertheussen, E.; Lin, J. C.; Davis, R. C.; Beeman, J. W.; Higgins, D.; Drisdell, W. S.; Hahn, C.; Mehta, A.; Seger, B.; Jaramillo, T. F.; Chorkendorff, I. Absence of Oxidized Phases in Cu under CO Reduction Conditions. *ACS Energy Lett.* **2019**, *4*, 803−804.
(70) Lum, Y.; Ager, J. W. Stability of Residual Oxides in Oxide-Derived Copper Catalysts for Electrochemical CO_2 Reduction Investigated with ^{18}O Labeling. *Angew. Chem., Int. Ed.* **2018**, *57*, 551−554.

https://doi.org/10.1021/jacs.3c00467
J. Am. Chem. Soc. 2023, 145, 10116−10125